https://doi.org/10.48048/tis.2024.7078

# Preparation of Magnetic Activated Carbons from Cassava Peel using $H_3PO_4$ and KOH Activation by Microwave Heating for Naphthol Blue-Black Adsorption

**Widi Astuti[1,*], Irene Nindita Pradnya[1], Ria Wulansarie[1], Dhoni Hartanto[1], Triastuti Sulistyaningsih[2], Cepi Kurniawan[2], Miftakhul Hidayah[1], Lu'lu' Fitriana[1], Muhammad Arief Mahardhika[1] and Evin Fajri Irchamsyah[1]**

*[1]Department of Chemical Engineering, Universitas Negeri Semarang, Semarang 50229, Indonesia*
*[2]Department of Chemistry, Universitas Negeri Semarang, Semarang 50229, Indonesia*

**([*]Corresponding author's e-mail: widi_astuti@mail.unnes.ac.id)**

*Received: 12 May 2023, Revised: 18 June 2023, Accepted: 14 July 2023, Published: 20 November 2023*

**Abstract**

To address the separation problems and produce the reusable adsorbent, cassava peel magnetic activated carbon (MAC) prepared via microwave-assisted activation has been proposed to replace activated carbon (AC) for naphthol blue-black removal. To create MACs, ACs were embedded with nano-sized magnetite particles using co-precipitation methods. In this sense, 2 different activating agents (i.e., $H_3PO_4$ and KOH) have been used. $H_3PO_4$ activation provides a larger pore size and more functional groups, while KOH activation provides a larger surface area and higher porosity. The increase of $H_3PO_4$ concentration from 40 to 60 % leads to an increase in porosity as well as an increase in the weight ratio of KOH to char from 1 to 3. Impregnation magnetite to the ACs reduces surface area from 457.76 to 337.94 $m^2\ g^{-1}$ for KOH activation, and from 360.65 to 232.74 $m^2\ g^{-1}$ for $H_3PO4$ activation, decreasing adsorption capacity from 97.5 to 97 % for KOH activation and from 99 to 98 % for $H_3PO4$ activation. However, the adsorbent is easy to separate under the magnetic influence. The adsorption data of MAC by $H_3PO4$ activation show suitability with the Redlich-Peterson isotherm model, suggesting that naphthol blue-black removal is not ideal monolayer adsorption, but a combination of physisorption and chemisorption processes that exhibit heterogeneity of naphthol blue-black adsorption on the surface of adsorbent. Meanwhile, for MAC by KOH activation, the Langmuir isotherm is more suitable.

**Keywords:** Adsorption, Dye, Isotherm, Magnetization, Microwave heating

## Introduction

All societal strata in Indonesia value batik as a part of their national history. Batik preparation involves a dyeing procedure that is essential and important. In this process, synthetic dyes are frequently employed due to their vivid colors, accessibility, affordability, and easily bind to the hydroxyl groups of the cloth to form covalent bonds. There are 3 categories of dyes, namely anionic dyes (acid, reactive, azo, and direct dyes), cationic dyes (basic dyes), and non-ionic dyes (dispersion dyes). An azo dye used frequently by the textile industry for coloring textiles, nylon, silk, and batik is naphthol blue-black. The ionized aromatic chemical naphthol is more reactive than phenol. These organic substances are extremely poisonous, cancer-causing, and incapable of breaking down naturally [1]. Hence, it is urgent to reduce the dye before being discharged into the environment. Several treatment methods to remove the dye are expanded, including precipitation [2], membrane separation process [3], photocatalysis [4], and adsorption [5]. The precipitation method produces a large amount of toxic sludge that needs further chemical treatment and proper disposal. In addition, it lacks specificity and is ineffective for low concentrations [2]. Membrane technology cannot be carried out efficiently due to high operational costs, high energy consumption, and high concentration of sludge production [2]. Meanwhile, the photocatalytic method requires a significant amount of $O_2$, has a long duration time, and limited application [2]. Adsorption is most prominent due to its environmentally friendly, simple application, high efficiency, and low investment cost, especially if adsorbents are inexpensive and abundantly available. Several low-cost adsorbents have been studied by researchers such as bagasse-bentonite mixture [6], alga waste-bentonite mixture [7], and various types of activated carbon [8]. However, activated carbon (AC) is considered a pledge adsorbent to remove the dye from wastewater [8]. It is related to its large surface area, high porosity, surface chemistry properties related to the availability of functional groups, good thermostability, and high adsorption capacities [6]. However, the high

manufacturing cost causes the application of AC to be limited. To address this issue, many agricultural wastes have been utilized including peanut shell [9], pineapple crown leaf [10], and cassava stem [11]. Cassava (Manihot esculenta), a woody shrub perennial plant, commonly grows in tropical and subtropical regions, including Indonesia. Apart from being the main food, cassava is also widely used as a raw material in the food industry. In this sense, a large amount of cassava peel is produced and discharged into the environment as solid waste. The chemical content of cassava peel is 37.9 % cellulose, 23.9 % hemicellulose, and 7.5 % lignin [11], making it possible to act as a precursor in the AC preparation.

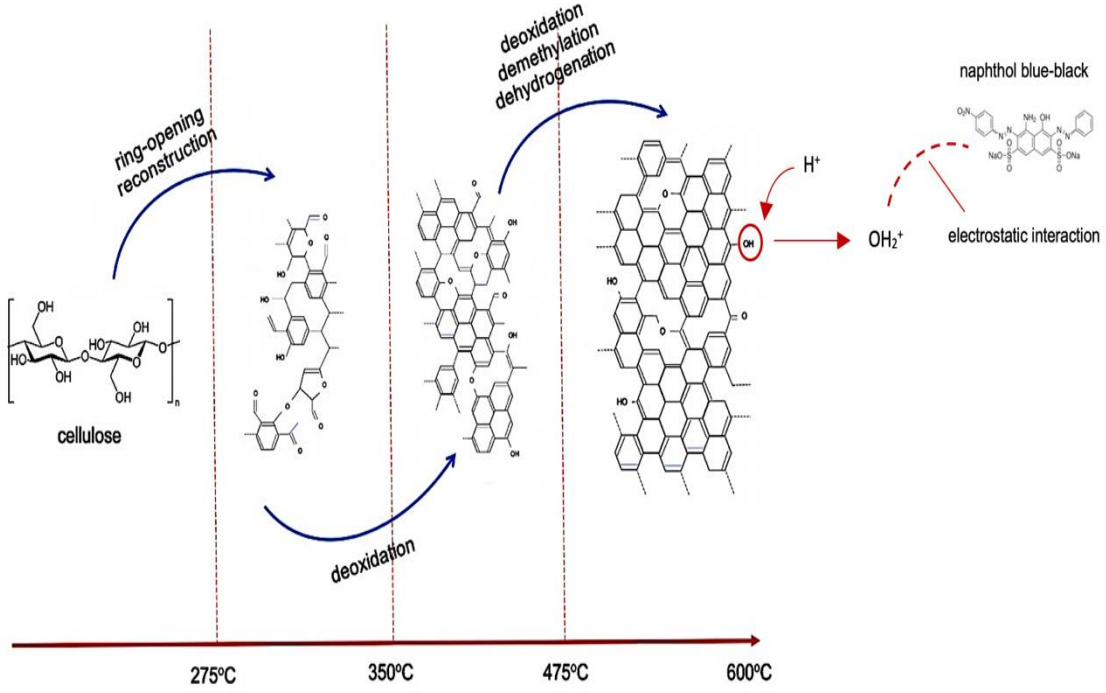


**Figure 1** Degradation reaction of cellulose to form biochar and adsorption mechanism of naphthol blue-black molecule on the adsorbent surface.

The production of AC from lignocellulosic sources such as agricultural waste and biomass is a 2-phase process, i.e., pyrolysis and activation. In the pyrolysis process, lignin, cellulose, and hemicellulose are degraded into biochar. Although the high pyrolysis temperature in the manufacture of biochar can destroy most of the organic functional groups derived from lignocellulosic material, biochar still contains various functional groups. As an example, the degradation reaction of cellulose to form biochar is presented in **Figure 1** [12]. Meanwhile, the activation process can be carried out in 2 ways, chemical activation and physical activation [13]. Although physical activation is a low-cost process with a lower environmental impact, chemical activation is preferred. Apart from opening blocked pores, widening existing pores, and forming new pores, the chemical activation process can also produce new functional groups, which will act as active sites in chemisorption, through electrostatic interactions (**Figure 1**) or the formation of other chemical bonds. In this case, the tunable pore structure, which is identified as porosity and specific surface area increases the accessibility of functional groups, while the dominant adsorption process occurs at the active sites. It is different from physisorption which occurs in pores through van der Waals forces, so the good adsorption capability of AC is related to its superior surface area, not its functional groups.

In chemical activation, the use of activating agents such as $H_3PO_4$ [14] and KOH [15] is generally preferred because it requires lower temperature, produces a higher yield, creates a better porous structure, and obtains materials having a larger surface area and more functional groups. In this sense, the use of microwave as a heating source is a promising alternative to replace conventional heating due to several advantages such as rapid temperature rise, leading to a faster process time and a decrease in energy consumption [16]. In addition, microwave heating creates a uniform temperature distribution, thereby reducing the temperature gradient in the material, leading to uniformity of the pore size [17]. Although AC can effectively remove various contaminants in wastewater, it has obstacles in the separation process. In

order to address the separation problems and produce the reusable adsorbent, the loading of nano-sized magnetite particles to the AC has been proposed [18]. Magnetite is an iron oxide containing both ferrous and ferric ions, providing magnetic properties to the activated carbon [18]. It allows activated carbon to be more easily separated from wastewater using a magnetic field. Therefore, the main objective of this research was to prepare cassava peel magnetic activated carbon to replace activated carbon for dye adsorption. The focus of this research is to compare the effectiveness of $H_3PO_4$ and KOH activation coupled with microwave heating. Furthermore, the effect of the activation mechanism on the pore structure and adsorption ability is analyzed and discussed. To the best of our knowledge, there isn't any literature that specifically reported a similar study, making this study a fascinating subject for further investigation.

## Materials and methods

### Materials

The cassava peel waste used in the study was obtained from a cassava chip factory in Gunungpati, Indonesia, which uses the Mangu variety with an average harvest age of 10 months. The waste was chopped into small pieces, washed, and dried at 110 ºC for 24 h in an electric oven (Memmert type UN55, Germany). Furthermore, dried cassava peel was ground to a fine powder.

### Preparation and characterization of activated carbon

The cassava peel powder was entered into an electric furnace (Model FB1310M-33 Thermolyne, Thermo Scientific, USA) at 700 ºC for 1 h in limited air for obtaining char. Furthermore, $H_3PO_4$ and KOH were used to investigate the effect of different activating agents on the characters of AC and MAC. For $H_3PO_4$ activation, 10 g of char was added to a 120 mL solution of $H_3PO_4$ with different concentrations (40, 50 and 60 %). The mixture was stirred for 24 h, filtered, and dried at 110 ºC for 24 h. The resulting ACs were denoted as ACP-40, ACP-50, and ACP-60, respectively. For KOH activation, 10 g of char was mixed with KOH and 10 mL of distilled water. In this sense, the weight ratio of KOH to char was set at 1, 2, and 3. The mixture was stirred for 24 h, filtered, and dried at 110 ºC for 24 h. The resulting ACs were denoted as ACK-1, ACK-2, and ACK-3, respectively. The impregnated chars were then placed in an alumina reactor and inserted in a 2.45 GHz microwave oven (Model ME731K Samsung, Malaysia with modification to minimize inconsistencies of microwave intensity during heating). Several modifications were made, including the use of 2 magnetrons and a double-wall reactor. In this case, the effect of power on the temperature profile and the characteristics of ACs has been published by Astuti *et al.* [19]. The heating is carried out at 600 W under a flow of $N_2$ of 0.25 L $min^{-1}$ for 7 min. After washing and the final drying stage, the ACs were embedded with nano-sized magnetite particles using co-precipitation methods [20]. MACs obtained from ACP-40, ACP-50, and ACP-60 were denoted as MACP-40, MACP-50, and MACP-60, respectively, while MACs obtained from ACK-1, ACK-2, and ACK-3 were denoted as MACK-1, MACK-2, and MACK-3, respectively. The surface area and pore radius of adsorbents were characterized by $N_2$ adsorption-desorption isotherm at 77 K, using an automated gas sorption apparatus QuantaChrome model Nova 1200 (USA) and calculated by Brunauer-Emmett-Teller (BET) equation for surface area and Barret-Joiner-Halenda (BJH) equation for pore radius. Scanning Electron Microscope (SEM) analysis with Phenom ProX Desktop (UK) was carried out on the adsorbents to study the surface morphology. The functional groups present in the adsorbents were evaluated by Fourier-transform infrared spectroscopy (FTIR) spectra (Perkin Elmer, USA), which were recorded between 500 and 4000 $cm^{-1}$ with the KBr disc method. To determine the $pH_{ZPC}$ of adsorbents, 0.15 g of adsorbent was added to the Erlenmeyer containing 50 mL NaCl 0.01 mol $L^{-1}$. HCl 0.1 mol $L^{-1}$ or NaOH 0.1 mol $L^{-1}$ were used to bring the pH of the solution to the desired pH range (2 - 12). The Erlenmeyers were then shaken at 200 rpm for 48 h at room temperature. Thereafter, the solution pH was measured using a pH meter. The pH data obtained were then curved toward the initial pH. The point of intersection between the final pH and initial pH is the $pH_{ZPC}$ value [21,22].

### Batch adsorption studies

Naphthol blue-black used as adsorbate has a molecular formula of $C_{22}H_{14}N_6Na_2O_9S_2$. For the experiment, a 1.0 g $L^{-1}$ naphthol blue-black stock solution was prepared by dissolving an appropriate amount of naphthol blue-black powder in distilled water. Batch adsorption studies were carried out by adding 0.3 g of adsorbent to 50 mL of naphthol blue-black solutions with different concentrations (10 - 500 mg $L^{-1}$). The solution pH was adjusted with the addition of 0.1 N HCl or 0.1 N NaOH to an appropriate pH (1, 3, 5, 7, 9, 11). The mixtures were further stirred at 120 rpm for 10 - 180 min. Then suspended solids were filtered and the filtrates were analyzed for residual naphthol blue-black using a UV-Visible spectrophotometer (Model Genesys 10 UV, Thermo Scientific, USA) at a wavelength ($\lambda$ max) of 595 nm.

The amount of naphthol blue-black uptake at equilibrium, $q_e$ (mg $g^{-1}$), was expressed according to the following equation [20]:

$$q_e = \frac{(C_o - C_e)\,V}{m} \quad (1)$$

with $C_o$ (mg $L^{-1}$) is the initial concentration of naphthol blue-black solution, $C_e$ (mg $L^{-1}$) is the concentration of naphthol blue-black in the solution at equilibrium, $m$ is adsorbent mass (g), and $V$ (L) is the volume of naphthol blue-black solution. While the maximum adsorbed naphthol blue-black at any time, $t$ (min) was determined in Eq. (2) as follows [20]:

$$q_t = \frac{(C_o - C_t)\,V}{m} \quad (2)$$

with $C_t$ (mg $L^{-1}$) is the concentration of naphthol blue-black in the solution at any time. The percentage of naphthol blue-black adsorbed on the adsorbents was expressed by Eq. (3) as follows [20]:

$$\text{naphthol blue-black adsorbed (\%)} = \frac{(C_o - C_t)}{C_o} \times 100 \quad (3)$$

## Results and discussion

### Characterization of adsorbents

The morphology of char prepared from cassava peel is presented in **Figure 2**. Char has a honeycomb pore skeleton with twisted walls and a cottony structure. However, most pores are blocked and filled by tarry pyrolysis residues formed during the carbonization process. Subsequent to the activation process using KOH coupled with microwave heating, many pores in a honeycomb-like shape are created. The use of microwaves in the activation process aims to reduce the temperature gradient in the material during conventional heating, which results in non-uniformity of the pore size. KOH can efficiently stimulate the gasification and cracking of organic components on the surface of biochar, producing a greater proportion of gaseous products and fewer volatiles. In reference to the KOH activation mechanism in Eqs. (4) - (8), more CO and $CO_2$ are produced [20].

$$2KOH \rightarrow K_2O + H_2O \quad (4)$$

$$C_f + H_2O \rightarrow H_2 + CO \quad (5)$$

$$CO + H_2O \rightarrow H_2 + CO_2 \quad (6)$$

$$K_2O + C_f \rightarrow 2K + CO \quad (7)$$

$$K_2O + H_2 \rightarrow 2K + H_2O \quad (8)$$

$$K_2O + CO_2 \rightarrow K_2CO_3 \quad (9)$$

Concurrently, $K_2CO_3$ that was created by the reaction in Eq. (9) was reduced in an inert condition to generate CO, $CO_2$, $K_2O$, and K as a final product, according to the following reaction [20]:

$$K_2CO_3 + 2C_f \rightarrow 2K + 3CO \quad (10)$$

$$K_2CO_3 \rightarrow K_2O + CO_2 \quad (11)$$

$$K_2O + C_f \rightarrow 2K + CO \quad (12)$$

According to Eqs. (10) - (12), it is deduced that the potassium (K) element was produced after a series of reactions in the activation process with KOH. The heat energy absorbed by K atoms impregnated in the carbon matrix causes the atoms to become energized. They can migrate and penetrate between graphene layers, enlarging the existing pores. Further heating at a temperature of around 800 ºC releases the atoms from the char matrix through the vent of the microwave oven. In this sense, K atoms function as a template

to widen the existing pores [20]. Accordingly, the increase in weight ratio from 1 (i.e., ACK-1) to 3 (i.e., ACK-3) leads to an increase in AC porosity, as can be seen in **Figure 2**. In addition, the use of KOH as an activating agent causes the formation of new pores. It is identified through a decrease in the pore diameter from 2.32 nm for char to 1.83 nm for ACK-3 (**Table 1**). The magnetization process leads to the surface of the activated carbon being partially covered with magnetite particles, as can be seen in **Figure 2(e)**. As a result, the surface area decreases from 457.76 to 337.94 $m^2 g^{-1}$ (**Table 1**).

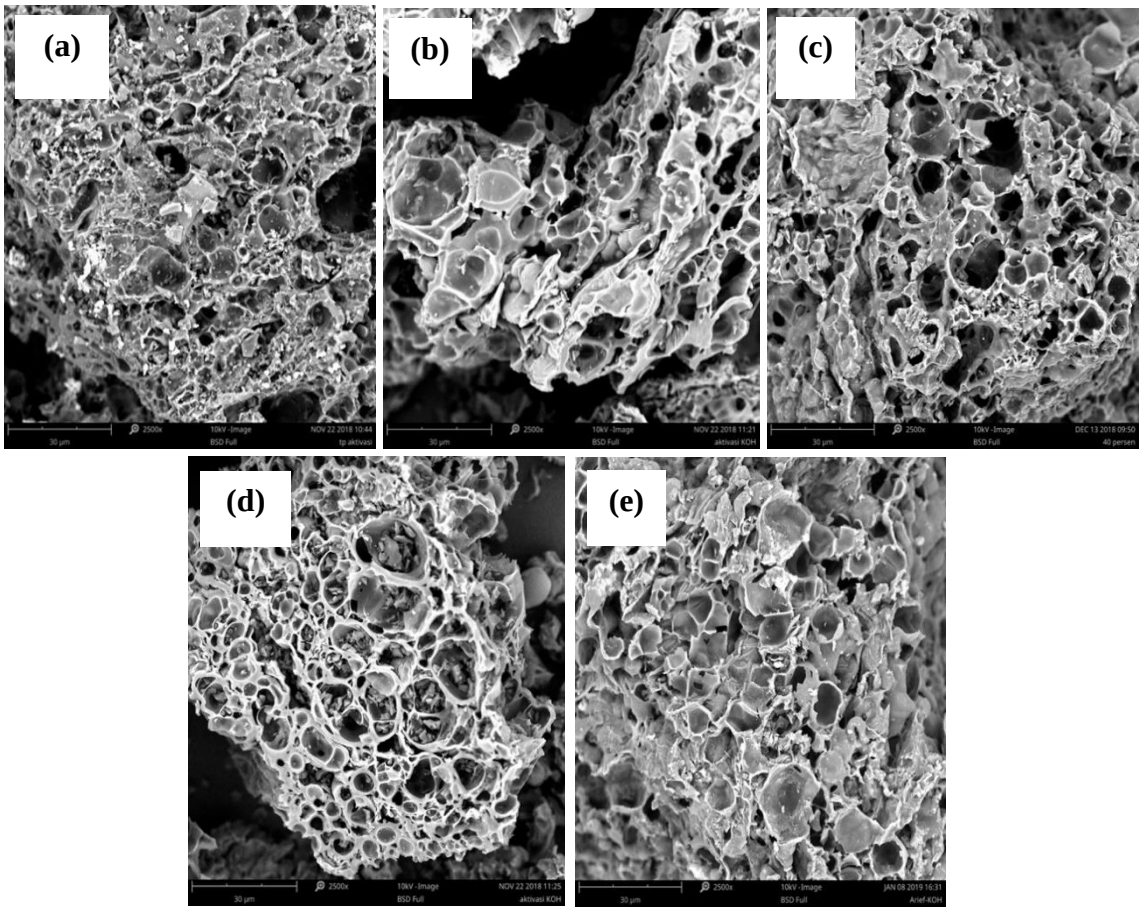


**Figure 2** SEM micrograph of (a) char, (b) ACK-1, (c) ACK-2, (d) ACK-3 (e) MACK-3.

**Table 1** Surface physical characteristics of adsorbents.

| Parameters | Char | ACK-3 | ACP-60 | MACK-3 | MACP-60 |
|---|---|---|---|---|---|
| BET surface area ($m^2 g^{-1}$) | 7.14 | 457.76 | 360.65 | 337.94 | 232.74 |
| Pore radius (nm) | 2.32 | 1.83 | 3.42 | 1.51 | 2.34 |
| Micropore volume (mL $g^{-1}$) | 0.0027 | 0.052 | 0.027 | 0.073 | 0.045 |
| Micropore volume (%) | 8.42 | 45.31 | 27.52 | 64.21 | 49.63 |

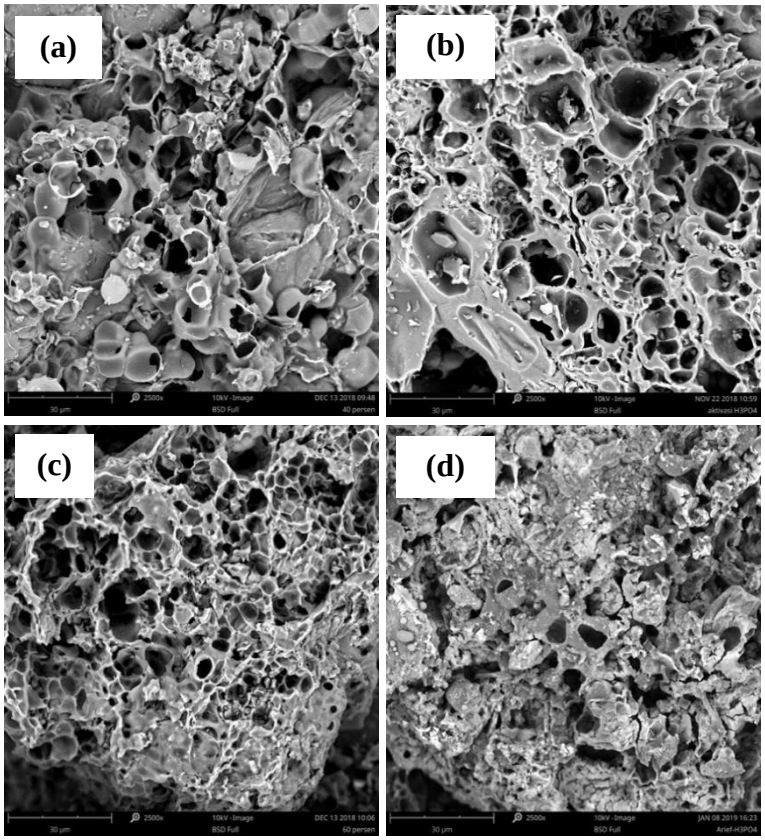


**Figure 3** SEM micrograph of (a) ACP-40, (b) ACP-50, (c) AC)-60 (e) MACP-60.

The morphology of activated carbon prepared using $H_3PO_4$ is presented in **Figure 3**. According to the figure, ACP has a wider pore size range with several large pores. $H_3PO_4$ acts as a cleaning and dehydrating agent to remove tarry products in the pores of char. Moreover, it promotes the breaking of aryl ether linkages, followed by chain damage, structure expansion, carbon redistribution, and phosphate polymerization, following Eqs. (13) - (15) [8]. As a result, the pore size increases from 2.32 to 3.42 nm (**Table 1**). However, this mechanism is ineffective in releasing tarry substances from the pores, and as a consequence of that, several pores still appear clogged. The increase of $H_3PO_4$ concentration from 40 (i.e., ACP-40) to 60 (i.e., ACP-60) leads to an increase in AC porosity. When nano-sized magnetite particles are embedded in the activated carbon, more pores are blocked and covered by magnetite (**Figure 3(d)**). Comparing MACP to MACK, some of the MACP pore framework is unclear. Moreover, the remaining pores have thick walls. It may be due to the fact that there are still many ACP pores filled with tar, so during the magnetization process, only a few nano-sized magnetite particles can diffuse into the ACP pores and the rest cover the ACP surface, resulting in a denser surface.

$$4\ H_3PO_4 + 10\ C \rightarrow P_4 + 10\ CO + 6\ H_2O \quad (13)$$

$$4\ H_3PO_4 \rightarrow P_4O_{10} + 6\ H_2O \quad (14)$$

$$P_4O_{10} + 10\ C \rightarrow P_4 + 10\ CO \quad (15)$$

In order to investigate the chemical properties of the chars, ACs, and MACs, FT-IR analysis was performed. The results are presented in **Figure 4**. The spectrum of char showed a broad absorption band at 3500 $cm^{-1}$ extending to 3700 $cm^{-1}$, with a more evident peak at 3647 $cm^{-1}$ is ascribed to O-H stretching vibrations present in the structure of cellulose, hemicellulose, and lignin [23]. As previously explained, biochar produced from biomass contains functional groups derived from lignin, cellulose, and hemicellulose, albeit the majority of the organic functional groups can be lost during the high-temperature pyrolysis process. The degradation reaction of lignin, cellulose, and hemicellulose during the pyrolysis

process to form char has been described in detail by Liu *et al.* [12]. The spectral band in the range of 1600 - 1700 $cm^{-1}$ can be attributed to the C=O stretching vibration of ketone, lactone, aldehyde, and carboxyl groups found in cellulose [23]. The band between 1500 and 1600 $cm^{-1}$, with a peak at 1527 $cm^{-1}$ is the unsaturated stretching of C-C bonds ascribed to aromatic C=C vibration, typical of carbonaceous materials. The band at ca. 1000 - 1050 $cm^{-1}$, with a peak at 1042 $cm^{-1}$ probably due to the R-OH groups [24]. After the activation process, an increase or a decrease in peak intensity related to the surface functional groups existing in the ACs is observed, as well as the appearance of new functional groups. Peak around 3400 - 3700 $cm^{-1}$ is deeper, suggesting the increase of hydroxyl groups. Comparing the ACP with ACK, the intensity of this peak in ACP is higher than that of ACK, relating to the acidity of the adsorbent [25]. The high intense band at 1000 - 1250 $cm^{-1}$ observed in the ACP spectrum is probably caused by the phosphate group since it revealed the P=O stretching vibration, O-C stretching vibration in the P-O-C linkage, P=OOH, and stretching vibration in P-O-P polyphosphate chains [24]. It indicates the formation of carbon-oxygen groups accompanying the increase of phosphorus-containing groups [24]. The band at 1500 - 1600 $cm^{-1}$ decreases, evidencing the cracking of the C=C bond during the activation process. The embedding of magnetite particles in the ACs leads to a decrease in the intensity of the band at 3500 - 3700 $cm^{-1}$, while a new peak appears at approximately 600 $cm^{-1}$ indicating the existence of the Fe-O group [20].

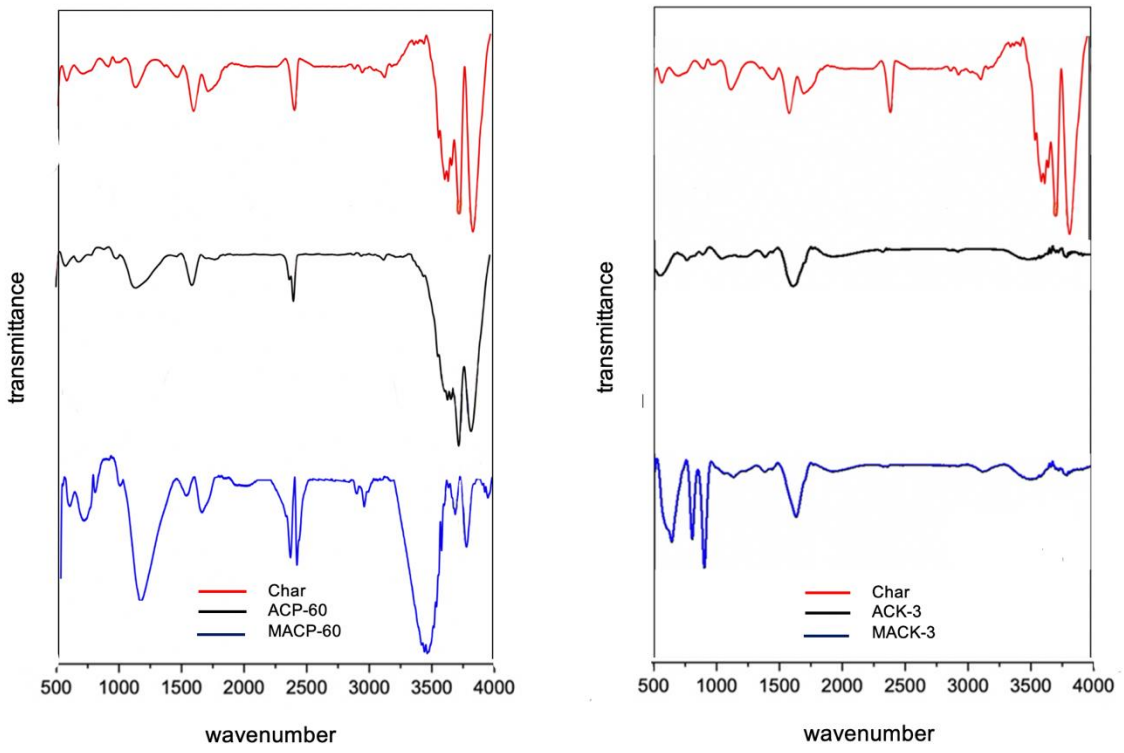


**Figure 4** FTIR spectra of (a) char, ACP-60, and MACP-60, and (b) char, ACK-3, and MACK-3.

**Adsorption performance**

The effect of the impregnation ratio on the naphthol blue-black adsorption is described in **Figure 5(a)**. An increase in the weight ratio of KOH to char from 1 to 3 leads to an increase in the amount of naphthol blue-black adsorbed on the ACs. It may be due to the increase in the porosity of ACs, resulting in increases in the accessibility of functional groups. The same result was attained for AC using $H_3PO_4$ as an activating agent (**Figure 5(b)**). The increase in $H_3PO_4$ concentration leads to an increase in the amount of dye adsorbed. Generally, the amount of naphthol blue-black adsorbed on the ACP is higher than the amount of naphthol blue-black adsorbed on the ACK due to more functional groups in the ACP. In this sense, the adsorption mechanism is more appropriate with chemisorption through electrostatic interaction than physisorption, since only 1.6 - 3.2 % naphthol blue-black can be desorbed from ACs by distilled water. The loading of nano-sized magnetite particles to the ACs slightly decreases the amount of naphthol blue-black

adsorbed (**Figure 5(c)**) due to some of the pores being covered and blocked by magnetite particles, leading to a decrease in the amount of accessible functional group. However, the decrease is insignificant while MAC has the advantage of being easily separated under a magnetic influence.

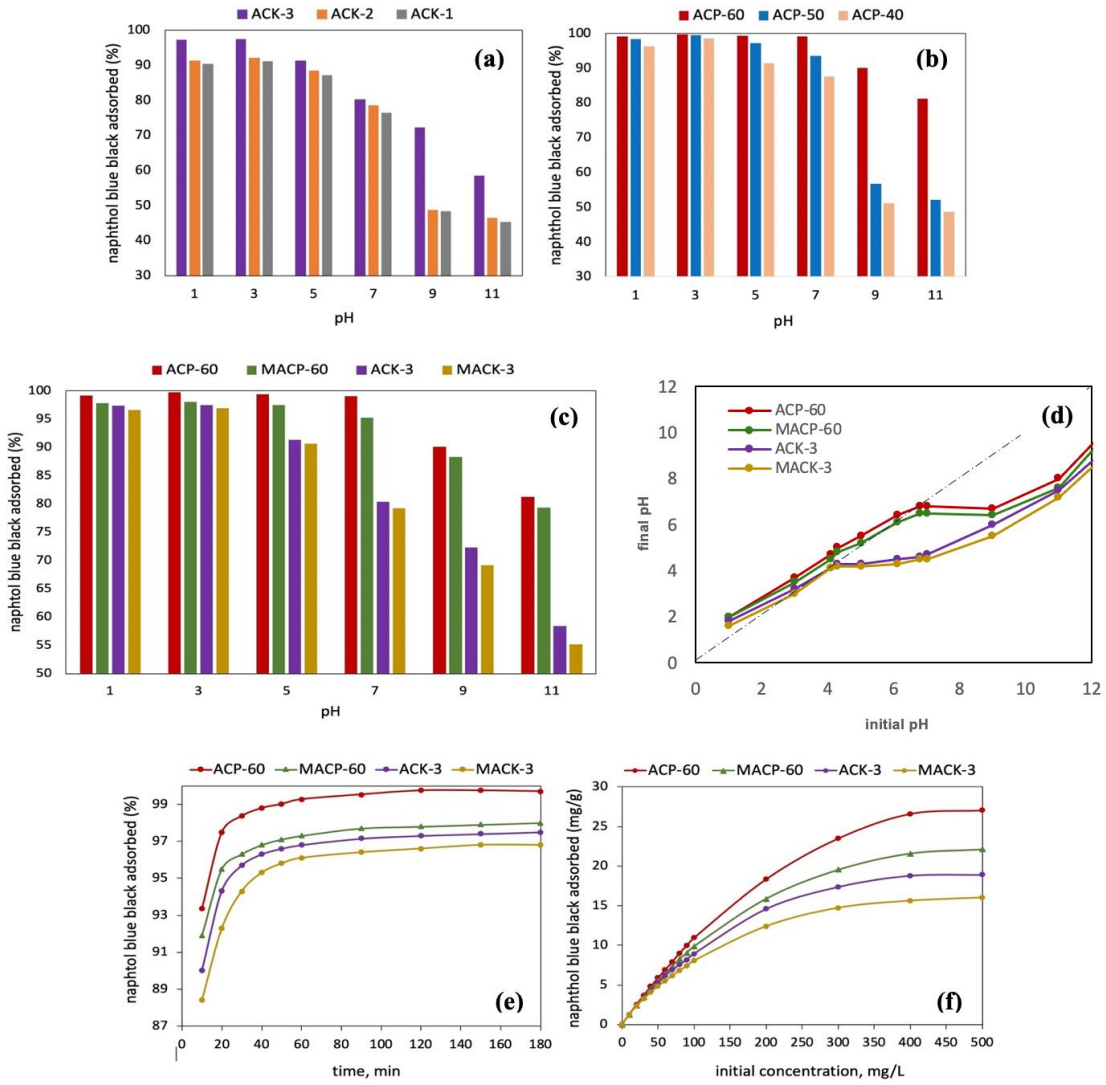


**Figure 5** (a) Effect of pH on the amount of naphthol blue-black adsorbed at various $H_3PO_4$ concentrations, (b) Effect of pH on the amount of naphthol blue-black adsorbed at various weight ratios of KOH to char, (c) Effect of pH on the amount of naphthol blue-black adsorbed at various adsorbents, (d) $pH_{ZPC}$ of ACs and MACs, (e) Effect of adsorption time on the amount of naphthol blue-black adsorbed, and (f) Effect of initial concentration on the amount of naphthol blue-black adsorbed (activated carbon dosage of 0.2 g / 25 mL dye solution).

The $pH_{ZPC}$ is a very important parameter in the characterization of the activated carbons, which indicates the acid-base behavior of the adsorbent surface. **Figure 5(d)** shows the $pH_{ZPC}$ of ACP-60, MACP-60, ACK-3, and MACK-3 is 6.5, 6.1, 4.3, and 4.1, respectively. These values indicate that the activated carbons produced have an acidic character. At pH less than $pH_{ZPC,}$ the surface of the adsorbent is protonated according to $-COH + H^+ \rightarrow -COH_2^+$, indicating a positively charged surface group. While at a pH larger than $pH_{ZPC}$, the hydroxyl group could dissociate according to $-COH \rightarrow CO^- + H^+$, representing a negatively charged surface group. It indicates that the increase in pH leads to a change in the surface charge from positive to negative. As naphthol blue-black is an anionic dye having a negative charge, the increase in pH leads to electrostatic repulsion between active sites (i.e., functional groups) in the adsorbent surface and

adsorbate molecules (i.e., naphthol blue-black). As a result, the amount of naphthol blue-black adsorbed decreases (**Figure 5(c)**).

**Figure 5(e)** shows the quantity of naphthol blue-black adsorbed on the ACs and MACs increase rapidly in the first 10 min and slower near equilibrium. It may be due to a large number of vacant sites available for adsorbing naphthol blue-black during the initial stage. Subsequent to the active site being occupied during the adsorption process, the diffusion of naphthol blue-black molecules to the remaining active sites is inhibited due to the repulsive forces of the adsorbed molecules [25]. It is observed that adsorption equilibrium was reached at 150 min (for ACP and MACP) and 120 min (for ACK and MACK). This finding contradicts previous studies which stated that a larger surface area gives a longer time to reach equilibrium due to more dye molecules can be adsorbed [25]. In this study, MACK having a higher surface area than MACP reached equilibrium faster. It may be due to the greater number of functional groups in MACP than in MACK. The functional groups act as active sites in the chemisorption of naphthol blue-black onto MACs and ACs.

The effect of initial concentration on the naphthol blue-black uptake is presented in **Figure 5(f)**. The amount of dye adsorbed increases with the increase in initial dye concentration, and then it gradually slows down. The initial dye concentration provides a driving force to overcome all mass transfer resistance in the adsorption process [19]. In addition, **Figures 5(e)** and **5(f)** also show that embedding magnetite to the AC decreases the amount of naphthol blue-black adsorbed, although the decrease is insignificant.

**Adsorption isotherm**

To define how the adsorbate species attaches to the surface of the adsorbent, adsorption isotherm analysis is crucial. The equation parameters of these isotherm models often provide some insight into the adsorption mechanism, the surface properties, and the affinity of the adsorbent for the adsorbate. The isotherm model used in this study focuses on comparing localized adsorption on homogeneous and heterogeneous adsorbent surfaces. Therefore, 3 types of isotherm models namely Langmuir, Freundlich, and Redlich-Peterson are considered for isotherm investigation. Langmuir isotherm follows the assumption that all adsorption sites on the adsorbent surface are homogeneous, i.e., equal in size and energy. This model applies to localized adsorption of monolayer surface coverage assuming that each site only can bind one adsorbate molecule and no interaction between adsorbate molecules. No more adsorption can take place on the adsorbent surface after the monolayer is full. Meanwhile, the Freundlich isotherm presupposes that adsorption occurs on heterogeneous surfaces with various adsorption energies and heterogeneous binding sites. In this sense, weak Van der Waals forces between adsorbate molecules might cause multilayer adsorption on the adsorbent surface. Different from Langmuir and Freundlich which is a two-parameter isotherm model, Redlich-Peterson is a 3-parameter isotherm model that combines the features of the Freundlich and Langmuir isotherms that serve to address the limitations of individual models. It will be compared and studied further in this study. Redlich-Peterson model does not represent ideal monolayer adsorption but rather a combination of physisorption and chemisorption processes which highlight the heterogeneity of adsorption on the adsorbent surface. Due to its adaptability, this isotherm model can depict properly adsorption equilibrium conditions over a wide concentration range of adsorbate. Redlich-Peterson isotherm reduces to the Freundlich model at high adsorbate concentrations, when the exponent β approaches zero and $\alpha_R$ is greater than 1. For low concentration, it simplifies to the Langmuir model, owing to the fact that the β value approaches one. The Langmuir isotherm can be expressed as [20]:

$$q_e = q_m \frac{K_L C_e}{1 + K_L C_e} \tag{16}$$

where $q_m$ is the Langmuir maximum adsorption capacity of the adsorbent (mg $g^{-1}$) and $K_L$ (L $mg^{-1}$) is the Langmuir constant related to the adsorption energy. Eq. (16) is solved by optimizing the correlation coefficient between the value of $q_e$ data and $q_e$ predicted from Eq. (16). The isotherm parameters are observed using the solver add-in feature of Microsoft Excel software by minimizing the difference between the experimental data and the model. The Freundlich isotherm is formulated as [20]:

$$q_e = K_F C_e^{\frac{1}{n}} \tag{17}$$

with $K_F$ ($mg^{1-1/n}\ g^{-1}\ L^{1/n}$) is the Freundlich constant related to the adsorption capacity, while *1/n* is the Freundlich exponent related to the adsorption intensity or the bonding energy between the adsorbate molecules and the adsorbent. The parameters in Eq. (17) are observed by optimizing the correlation

coefficient between the value of $q_e$ data and $q_e$ predicted from Eq. (17) using the solver add-in feature of Microsoft Excel software. The Redlich-Peterson isotherm is defined as [26]:

$$q_e = \frac{K_R C_e}{1+ \alpha_R C_e^{\beta}} \tag{18}$$

where $K_R$ (L $g^{-1}$) and $\alpha_R$ ((L $mg^{-1})^{\beta}$) are the constants of the Redlich-Peterson isotherm while β is the Redlich-Peterson isotherm exponent having a value between 0 and 1. The parameters in Eq. (18) are observed by optimizing the correlation coefficient between the value of $q_e$ data and $q_e$ predicted from Eq. (18) using the solver add-in feature of Microsoft Excel software.

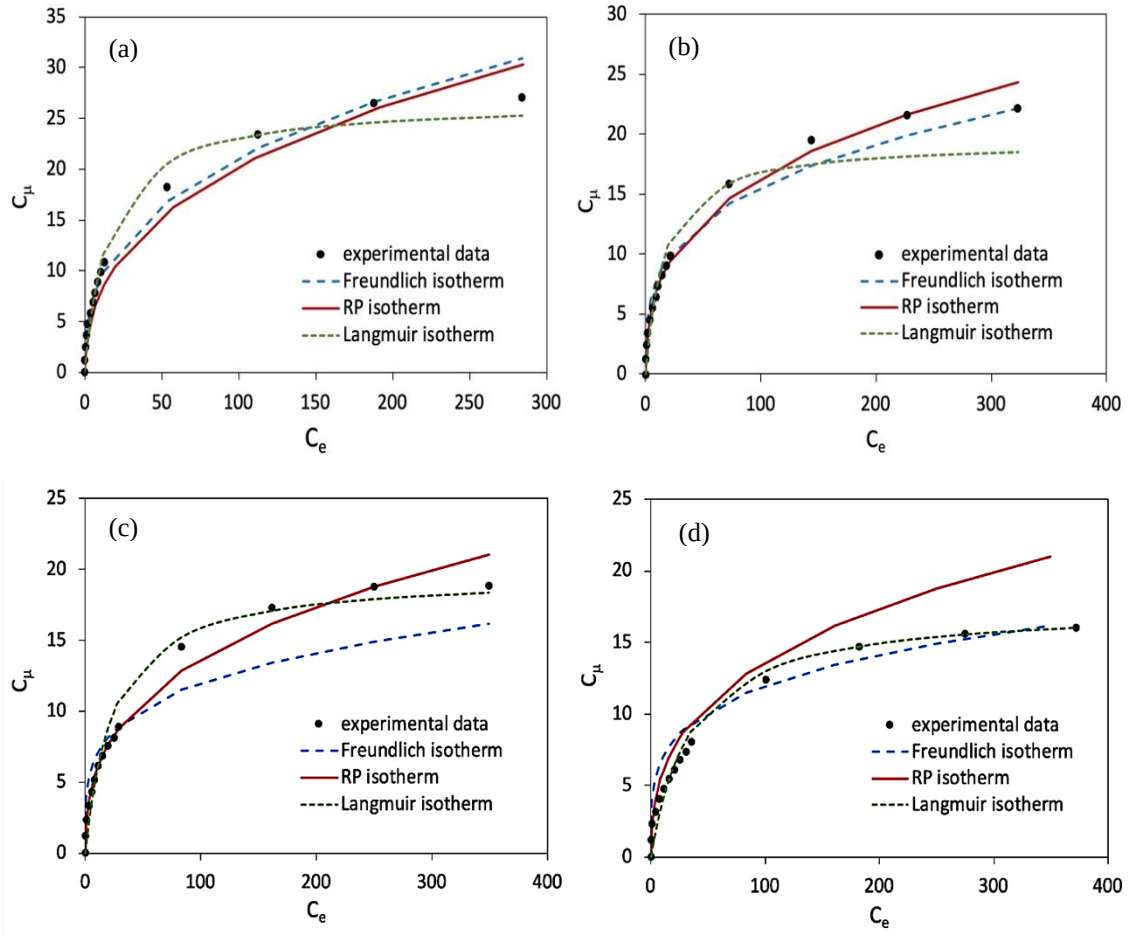


**Figure 6** Isotherm adsorption for (a) naphthol blue-black-ACP-60 system, (b) naphthol blue-black-MACP-60 system, (c) naphthol blue-black-ACK-3 system, (d) naphthol blue-black-MACK-3 system.

The sum of the square of the errors (SSE), non-linear chi-square test ($\chi^2$), and average relative error (ARE) are used to estimate the validity of the models. They are defined as [20]:

$$SSE = \sum_{i=1}^{N}\left(q_{e,calc} - q_{e,meas}\right)^2 \tag{19}$$

$$\chi^2 = \sum_{i=1}^{N}\left(q_{e,calc} - q_{e,meas}\right)^2 / q_{e,meas} \tag{20}$$

$$ARE = \frac{100}{N}\sum_{i=1}^{N}\left|\left(q_{e,calc} - q_{e,meas}\right)/q_{e,meas}\right| \tag{21}$$

where $q_{e,meas}$ is the value of $q_e$ measured from the experiment, $q_{e,calc}$ is the value of $q_e$ calculated from the isotherm models, and $N$ is the number of measurements.

Data in **Figure 6** and **Table 2** describing the nonlinear fit of experimental data using the Langmuir, Freundlich, and Redlich-Peterson isotherm models show different results for each adsorbent. For ACP-60 and MACP-60, it can be seen that the Redlich-Peterson model best fitted the experimental data because it has the lowest error function value. It suggested that naphthol blue-black removal is not ideal monolayer adsorption, but a combination of physisorption and chemisorption processes that exhibit heterogeneity of naphthol blue-black adsorption on the surface of ACP-60 and MACP-60 surfaces. It also indicates a hybrid adsorption mechanism allows Freundlich isotherm at high concentrations and allows Langmuir isotherm at low concentrations, as can be seen in **Figures 6(a)** and **6(b)**. Meanwhile, for ACK-3 and MACK-3, the Langmuir isotherm is more suitable. Data in **Figure 6** also shows that the adsorption capacity of ACP-60 is the highest. Nevertheless, embedding magnetite into the AC increases the separation efficiency, as previously described.

**Table 2** Isotherm parameters and values of error functions for naphthol blue-black-AC system naphthol blue-black-MAC system.

| Adsorbent | Langmuir isotherm | Freundlich isotherm | R-P isotherm |
|---|---|---|---|
| ACP-60 | $q_m$ = 26.72 | *1/n* = 0.36 | $\alpha_R$ = 1.52 |
| | $K_L$ = 0.06 | $K_F$ = 3.98 | $K_R$ = 5.79 |
| | SSE = 29.90 | SSE = 20.65 | $\beta$ = 0.63 |
| | $\chi^2$ = 6.24 | $\chi^2$ = 1.04 | SSE = 19.62 |
| | ARE = 23.85 | ARE = 6.99 | $\chi^2$ = 0.93 |
| | | | ARE = 3.82 |
| MACP-60 | $q_m$ = 19.59 | *1/n* = 0.29 | $\alpha_R$ = 1.52 |
| | $K_L$ = 0.06 | $K_F$ = 3.78 | $K_R$ = 5.71 |
| | SSE = 38.54 | SSE = 21.71 | $\beta$ = 0.62 |
| | $\chi^2$ = 4.08 | $\chi^2$ = 3.93 | SSE = 8.29 |
| | ARE = 19.39 | ARE = 20.24 | $\chi^2$ = 0.88 |
| | | | ARE = 8.21 |
| ACK-3 | $q_m$ = 19.39 | *1/n* = 0.24 | $\alpha_R$ = 1.42 |
| | $K_L$ = 0.04 | $K_F$ = 3.63 | $K_R$ = 5.67 |
| | SSE = 9.47 | SSE = 63.09 | $\beta$ = 0.61 |
| | $\chi^2$ = 0.79 | $\chi^2$ = 8.64 | SSE = 14.21 |
| | ARE = 6.91 | ARE = 29.95 | $\chi^2$ = 3.19 |
| | | | ARE = 18.11 |
| MACK-3 | $q_m$ = 17.51 | *1/n* = 0.214 | $\alpha_R$ = 1.40 |
| | $K_L$ = 0.03 | $K_F$ = 3.53 | $K_R$ = 5.61 |
| | SSE = 8.85 | SSE = 63.11 | $\beta$ = 0.61 |
| | $\chi^2$ = 0.71 | $\chi^2$ = 8.52 | SSE = 9.42 |
| | ARE = 6.81 | ARE = 29.11 | $\chi^2$ = 3.17 |
| | | | ARE = 16.26 |

**Table 3** The % removal of naphthol blue-black of some materials.

| Adsorbents | % Removal | Reference |
|---|---|---|
| mesoporous $TiO_2$ | 85.0 | [27] |
| Fe-doped $TiO_2$ | 90.1 | [28] |
| polyaniline-coated $TiO_2$ | 99.7 | [29] |
| MACK-3 | 97.0 | this work |
| MACP-60 | 98 | this work |

The ability of MACP-60 to remove naphthol blue-black is greater than that of MACK-3, although the surface area of MACP-60 (232.74 $m^2$) is lower than that of MACK-3 (337.94 $m^2$). It is presumably due to the role of the active site originating from P=O and P-O-C, as identified through the FTIR spectra. In this case, the adsorption mechanism follows the chemisorption through electrostatic interactions between dye molecules and the active sites. However, the physisorption via van der Waals bonds also occurs, especially at high concentrations, so the Redlich-Peterson isotherm model is more suitable. Whereas, for ACK-3 and MACK-3, the limitation of functional groups causes equilibrium to be reached more quickly and after the monolayer layer is full, no more dye molecules can be adsorbed, so the Langmuir model is more suitable.

According to a literature review, naphthol blue-black removal using other adsorbents such as mesoporous $TiO_2$ [27], Fe-doped $TiO_2$ [28], and polyaniline-coated $TiO_2$ [29] has also been studied as presented in **Table 3**. Thus, referring to **Table 3**, all MACs studied in this work appear to be compatible or better than other adsorbents, making a promising adsorbent for naphthol blue-black removal in an aqueous solution.

## Conclusions

The magnetic activated carbon (MAC) produced from cassava peel using microwave heating can be a promising alternative for dye removal. In this sense, $H_3PO_4$ activation provides a larger pore size and more functional groups, while KOH activation provides a larger surface area and higher porosity. The ability of MACP to remove naphthol blue-black is greater than that of MACK. The adsorption data of ACP-60 and MACP-60 show suitability with the Redlich-Peterson isotherm model, while, for ACK-3 and MACK-3, the Langmuir isotherm is more suitable.

## Acknowledgment

The authors are grateful to the Directorate of Research, Technology and Community Service, Ministry of Education, Culture, Research, and Technology of the Republic of Indonesia for the financial support of this work (Grant number: 038/E5/PG.02.00.PT/2022).

## References

[1] M Rezazadeh, M Baghdadi, N Mehrdadi and MA Abdoli. Adsorption of crystal violet dye by agricultural rice bran waste: Isotherms, kinetics, modeling and influencing factors. *Environ. Eng. Res*. 2021; **26**, 200128.

[2] R Shrestha, S Ban, S Devkota, S Sharma, R Joshi, AP Tiwari, HY Kim and MK Joshi. Technological trends in heavy metals removal from industrial wastewater: A review. *J. Environ. Chem. Eng.* 2021; **9**, 105688.

[3] S Zhang, S Liao, F Qi, R Liu, T Xiao, J Hu, K Li, R Wang and Y Min. Direct deposition of two-dimensional MXene nanosheets on commercially available filter for fast and efficient dye removal. *J. Hazard. Mater.* 2020; **384**, 121367.

[4] P Pascariu, C Cojocaru, N Olaru, P Samoila, A Airinei, M Ignat, L Sacarescu and D Timpu. Novel rare earth (RE-La, Er, Sm) metal doped ZnO photocatalysts for degradation of Congo-Red dye: Synthesis, characterization and kinetic studies. *J. Environ. Manag.* 2019; **39**, 225-34.

[5] YAB Neolaka, Y Lawa, J Naat, AC Lalang, BA Widyaningrum, GF Ngasu, KA Niga, H Darmokoesoemo, M Iqbal and HS Kusuma. Adsorption of methyl red from aqueous solution using bali cow bones (bos javanicus domesticus) hydrochar powder. *Results Eng*. 2023; **17**, 100824.

[6] EP Kuncoro, DRM Isnadina, H Darmokoesoemo, OR Fauziah and HS Kusuma. Characterization, kinetic, and isotherm data for adsorption of $Pb^{2+}$ from aqueous solution by adsorbent from mixture of bagasse-bentonite. *Data Brief* 2018; **16**, 622-9.

[7] EP Kuncoro, T Soedarti, TWC Putranto, H Darmokoesoemo, NR Abadi and HS Kusuma. Characterization of a mixture of algae waste-bentonite used as adsorbent for the removal of $Pb^{2+}$ from aqueous solution. *Data Brief* 2018; **16**, 908-13.

[8] YAB Neolaka, AAP Riwu, UO Aigbe, KE Ukhurebor, RB Onyancha, H Darmokoesoemo and HS Kusuma. Potential of activated carbon from various sources as a low-cost adsorbent to remove heavy metals and synthetic dyes. *Results Chem*. 2023; **5**, 100711.

[9] D Garg, S Kumar, K Sharma and CB Majumder. Application of waste peanut shells to form activated carbon and its utilization for the removal of acid yellow 36 from wastewater. *Groundwater Sustain. Dev*. 2019; **8**, 512-9.

[10] W Astuti, T Sulistyaningsih, D Prastiyanto, BSA Purba and R Kusumawardani. Synthesis of magnetically separable activated carbon from pineapple crown leaf for zinc ion removal. *Mater. Sci. Forum* 2020; **1007**, 71-5.
[11] NS Sulaiman, R Hashim, MHM Amini, M Danish and O Sulaiman. Optimization of activated carbon preparation from cassava stem using response surface methodology on surface area and yield. *J. Cleaner Prod.* 2018; **198**, 1422-30.
[12] J Liu, X Chen, W Chen, M Xia, Y Chen, H Chen, K Zeng and H Yang. Biomass pyrolysis mechanism for carbon-based high-value products. *Proc. Combust. Inst*. 2023; **39**, 3157-81.
[13] Arnelli, WP Aditama, Z Fikriani and Y Astuti. Adsorption kinetics of surfactants on activated carbon. *IOP Conf. Ser. Mater. Sci. Eng.* 2018; **349**, 012023.
[14] C Saka, D Yildiz, S Kaya, A Caglar, D Elitok, E Yayli, M Kaya, R Atelge and H Kivrak. A novel hazelnutt bagasse based activated carbon as sodium borohydride methanolysis and electrooxidation catalyst. *Int. J. Hydrogen Energ.* 2023; **48**, 25339-53.
[15] O Oginni, K Singh, G Oporto, B Dawson-Andoh, L McDonald and E Sabolsky. Influence of one-step and two-step KOH activation on activated carbon characteristics. *Bioresource Tech. Rep.* 2019; **7**, 100266.
[16] HS Kusuma, A Altway and M Mahfud. Solvent-free microwave extraction of essential oil from dried patchouli (*Pogostemon cablin* benth) leaves. *J. Ind. Eng. Chem*. 2018; **58**, 343-8.
[17] G Qi, Z Pan, X Zhang, S Chang, H Wang, M Wang, W Xiang and B Gao. Microwave biochar produced with activated carbon catalyst: Characterization and adsorption of heavy metals. *Environ. Res.* 2023; **216**, 114732.
[18] KM Lompe, SV Duy, S Peldszus, B Sauvé and B Barbeau. Removal of micropollutants by fresh and colonized magnetic powdered activated carbon. *J. Hazard. Mater*. 2018; **360**, 349-55.
[19] W Astuti, T Sulistyaningsih, RM Ramadhan and VA Octaviany. Synthesis of activated carbon from petung bamboo stems (*Dendrocalamus Asper*) using microwave-assisted pyrolysis (MAP) process for biogas storage. *Jurnal Bahan Alam Terbarukan* 2022; **11**, 58-67.
[20] W Astuti, T Sulistyaningsih, E Kusumastuti, GYRS Thomas and RY Kusnadi. Thermal conversion of pineapple crown leaf waste to magnetized activated carbon for dye removal. *Bioresour. Tech.* 2019; **287**, 121426.
[21] EP Kuncoro, DRM Isnadina, H Darmokoesoemo, F Dzembarahmatiny and HS Kusuma. Characterization and isotherm data for adsorption of $Cd^{2+}$ from aqueous solution by adsorbent from mixture of bagasse-bentonite. *Data Brief* 2018; **16**, 354-60.
[22] YAB Neolaka, Y Lawa, J Naat, AAP Riwu, YE Lindu, H Darmokoesoemo, BA Widyaningrum, M Iqbal and HS Kusuma. Evaluation of magnetic material IIP@GO-$Fe_3O_4$ based on Kesambi wood (*Schleichera oleosa*) as a potential adsorbent for the removal of Cr(VI) from aqueous solutions. *Reactive Funct. Polymer*. 2021; **166**, 105000.
[23] A Chafidz, W Astuti, V Augustia, DT Novira and N Rofiah. Removal of methyl violet dye via adsorption using activated carbon prepared from *Randu* sawdust (*ceiba pentandra*). *IOP Conf. Ser. Earth Environ. Sci.* 2018; **167**, 012013.
[24] W Zhao, L Chen and Y Jiao. Preparation of activated carbon from sunflower straw through $H_3PO_4$ activation and its application for acid fuchsin dye adsorption. *Water Sci. Eng.* 2023; **16**, 192-202.
[25] MJP Brito, CM Veloso, LS Santos, RCF Bonomo and RCI Fontan. Adsorption of the textile dye Dianix® royal blue CC onto carbons obtained from yellow mombin fruit stones and activated with KOH and $H_3PO_4$: Kinetics, adsorption equilibrium and thermodynamic studies. *Powder Tech.* 2018; **339**, 334-43.
[26] W Astuti, T Sulistyaningsih and M Maksiola. Chemically modified kapok sawdust as adsorbent of methyl violet dye from aqueous solution. *Jurnal Teknologi* 2016; **78**, 35-42.
[27] Y Chang, X Liu, A Cai, S Xing and Z Ma. Glycine-assisted synthesis of mesoporous $TiO_2$ nanostructures with improved photocatalytic activity. *Ceram. Int.* 2014; **40**, 14765-8.
[28] DH Reddy, GK Dinesh, S Anandan and T Sivasankar. Sonophotocatalytic treatment of Naphthol Blue Black dye and real textile wastewater using synthesized Fe doped $TiO_2$. *Chem. Eng. Process. Process Intensification* 2016; **99**, 10-8.
[29] S Debnath, N Ballav, H Nyoni, A Maity and K Pillay. Optimization and mechanism elucidation of the catalytic photo-degradation of the dyes Eosin Yellow (EY) and Naphthol blue black (NBB) by a polyaniline-coated titanium dioxide nanocomposite. *Appl. Catal. B Environ.* 2015; **163**, 330-42.